17th World Conference on Earthquake Engineering, 17WCEE
Sendai, Japan - September 13th to 18th 2020

SEISMIC FRAGILITY OF A BUCKLING RESTRAINED BRACED STEEL ROCKING FRAME

A. Baker[(1)], D. Dowden[(2)]

[(1)] *Graduate Research Assistant, Michigan Technological University, ambaker1@mtu.edu*
[(2)] *Assistant Professor, Michigan Technological University, dmdowden@mtu.edu*
...

Abstract

Present seismic building codes only require life-safety for typical structures subjected to rare earthquake events. Past earthquakes have shown this to be effective, yet costly. Designing only to the performance objective of life-safety leads to severe structural damage after a design level event, likely requiring the demolition of the building. This design paradigm can leave urbanized regions vulnerable to significant economic and socioeconomic losses. Therefore, low- damage seismic force-resisting systems (SFRSs) that allow buildings to be easily repaired after a design level earthquake are needed to facilitate rapid recovery. Low-damage SFRSs typically comprise of self-centering systems that isolate energy dissipation to replaceable elements (i.e. structural fuses) and typically provide frame self-centering through post-tensioned rocking joint details. Towards an alternative design paradigm, this paper presents preliminary results of an alternative low-damage SFRS that combines the excellent energy dissipation of buckling restrained brace (BRB) structural fuses with a post-tensioned (PT) beam-to-column rocking joint steel boundary frame. This proposed SFRS has significantly greater energy dissipation, but reduced frame self-centering capability compared to typical low- damage SFRSs. A parametric study of PT parameters was conducted on 3- and 6- story prototype buildings, and the collapse and self-centering fragilities of the proposed SFRS were assessed with incremental dynamic analyses using the FEMA P-695 ground motion suite.

Keywords: resilience; seismic fragility; incremental dynamic analysis; self-centering; rocking frame

1. Introduction

Seismic design practice has been rapidly changing in past decades to include innovative seismic force-resisting systems (SFRSs). One such system that has gained significant traction is the Buckling Restrained Braced Frame (BRBF) [1, 2]. A BRBF is a type of concentrically braced frame with special brace elements, referred to as Buckling Restrained Braces (BRBs), that are capable of yielding in both tension and compression without buckling. Research demonstrating the substantial energy dissipation, large ductility capacity, and simplicity of installation have made BRBs an appealing choice for SFRS solutions.

However, there is a trade-off to significant energy dissipation capability in both tension and compression. BRBFs have been shown to be susceptible to large residual drifts, with average interstory residual drifts after a design event of approximately 0.5% [3, 4]. This study presents preliminary results of a proposed SFRS which utilizes BRBs as energy dissipating elements in a self-centering post-tensioned (PT) rocking boundary frame. Various PT configurations for the system were investigated through non-linear static and dynamic analyses, and collapse and self-centering fragilities were developed using the FEMA P-695 (P-695) methodology as a guiding framework [5].

2. Proposed System

A schematic of the proposed SFRS is presented in Fig. 1. The SFRS combines the recently proposed NewZ-BREAKSS (NZ) PT boundary frame [6], detailed with a top-flange rocking joint to prevent beam-growth during interstory drift with BRB structural fuses. The pinned brace connections are separate from the column to accommodate rocking joint gap opening and closing. For the condition shown in the figure, the PT elements are located at the beam centroid with anchorages at the column and at 1/3 points along the beam span.

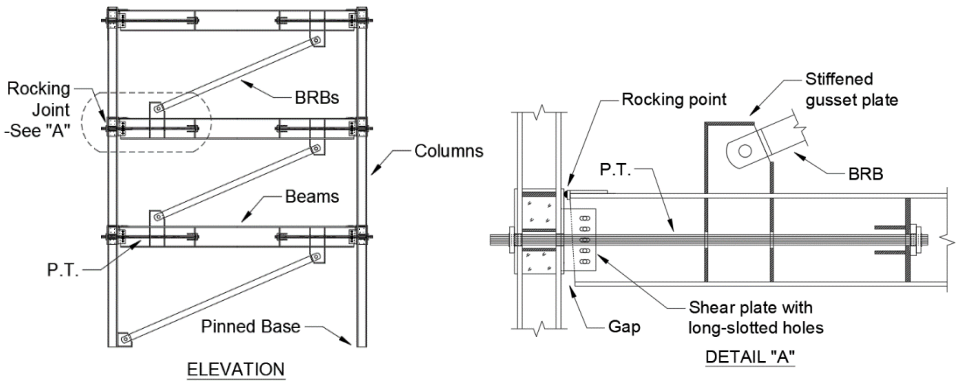

Fig. 1 – NZ-BRB Schematic Details

3. Building Designs

Following the P-695, prototype buildings were designed according to current building codes and design standards. The Equivalent Lateral Force (ELF) procedure per ASCE 7-16 [7] was selected as the design method for this study, as it is consistent with previous P-695 studies on BRBFs [8]. A preliminary response modification coefficient (i.e. *R*-factor) of 8, the code-based *R*-factor for BRBFs per ASCE 7-16, was assumed for the frame design.

The prototype buildings for this study used the 3-story benchmark building criteria from the SAC Steel Project [9]. The SAC buildings were developed to be typical of office buildings and have been widely used as benchmark buildings for other SFRSs [4, 10, 11]. The benchmark building is a 120 ft (36.6 m) by 180 ft (54.9 m) office building with a bay width of 30 ft (9.1 m) and a floor height of 13 ft (4.0 m). The building has a total of 12 braced bays, six in each direction. The floor and roof seismic masses are 65.53 kip-sec^2/ft (9.56 x 10^5 kg) and 70.9 kip-sec^2/ft (1.03 x 10^6 kg), respectively.

Using the same dimensions and seismic weights as the SAC 3-story building, 3-story and 6-story building designs were developed for this study. Each building was designed for the maximum ground motion parameters for ASCE 7-16 seismic design category D, and for 10% probability of collapse at the Maximum Considered Earthquake (MCE). A design story drift of 2% was assumed for the Design Basis Earthquake (DBE), and a target 4% interstory drift was assumed for frame strength design.

3.1 Buckling Restrained Braces

The BRBs were designed following NEHRP recommendations for BRB design [12]. The yielding core capacity was determined in accordance with AISC 341-16 [13], and required strength was determined from ELF base shear and distribution per ASCE 7-16, using approximate periods of 0.47 seconds for the 3-story prototype buildings and 0.79 seconds for the 6-story prototype buildings. The yielding cores of the braces were assumed to be A36 steel, with supplemental yield requirements of 42 +/- 4 ksi (290 +/- 28 MPa), as is common in practice [12, 14]. Since coupon tests were not available, the core areas were determined based on the assumed minimum specified yield stress of 38 ksi (262 MPa). The resulting BRB yielding core areas for the 3- and 6-story buildings are shown in Table 1.

Table 1 – BRB core areas, in^2 (mm^2)

	Floor					
Configuration	**1**	**2**	**3**	**4**	**5**	**6**
3-stories	4.50 (2903)	3.75 (2419)	2.25 (1452)			
6-stories	6.50 (4194)	6.50 (4194)	6.00 (3871)	5.00 (3226)	3.75 (2419)	2.25 (1452)

Overstrength on boundary frame members was calculated based on the adjusted strength of the BRBs, in accordance with AISC 341-16. The expected yield stress was taken to be the maximum specified yield stress of 46 ksi (317 MPa), and adjusted strength parameters were assumed to be $\omega = 1.4$ and $\beta = 1.1$ at the target interstory drift of 4% [12]. Brace stiffness was determined based on an assumed detailing of a yield zone length to work point length ratio of 0.5 and a stiffness modification factor of 1.7. Drift requirements were checked against the design story drift limit with the deflection amplification factor for BRBF systems per ASCE 7-16.

3.2 Post-Tensioning (PT)

PT strands were assumed to be 0.6 in (15.2 mm) diameter strands with an ultimate tensile stress of 270 ksi (1862 MPa) and a yield stress equal to 90% of the ultimate stress. For each building height, four configurations of PT were investigated, using the number of strands at each beam end and the ratio of initial stress to yield stress (σ_o/Fy) as parameters. A total of eight models were developed. For each model, the PT was designed to remain elastic at the target 4% interstory drift. The model IDs and PT parameters are summarized in Table 2.

Table 2 – PT Parameters

3-Stories			6-Stories		
ID	**Strands**	**σ_o/Fy**	**ID**	**Strands**	**σ_o/Fy**
3-14-15	14	0.15	6-14-15	14	0.15
3-14-30	14	0.30	6-14-30	14	0.30
3-22-15	22	0.15	6-22-15	22	0.15
3-22-30	22	0.30	6-22-30	22	0.30

3.3 Boundary Frame

The boundary frame was designed for strength and serviceability for gravity loads, as well as designed to remain elastic at the design level 2% drift. Furthermore, the boundary frame elements were capacity

designed for the adjusted BRB strength at the target 4% drift. AISC A992 wide-flange sections were used for all beams and columns, and resulting sizes are listed in Table 3 and Table 4.

Table 3 – Beam sizes

	Floor					
ID	**1**	**2**	**3**	**4**	**5**	**6**
3-14-15	W21X111	W21X101	W21X83			
3-14-30	W21X122	W21X122	W21X101			
3-22-15	W21X122	W21X122	W21X101			
3-22-30	W24X146	W24X146	W24X117			
6-14-15	W24X131	W24X131	W24X117	W24X117	W21X101	W21X83
6-14-30	W24X131	W24X131	W24X131	W24X117	W24X117	W21X101
6-22-15	W24X146	W24X131	W24X131	W24X117	W24X117	W21X101
6-22-30	W24X162	W24X162	W24X146	W24X146	W24X146	W24X117

Table 4 – Column sizes

	Floor					
ID	**1**	**2**	**3**	**4**	**5**	**6**
3-14-15	W14X61	W14X61	W14X61			
3-14-30	W14X82	W14X82	W14X82			
3-22-15	W14X90	W14X90	W14X90			
3-22-30	W14X132	W14X132	W14X132			
6-14-15	W14X132	W14X132	W14X90	W14X90	W14X61	W14X61
6-14-30	W14X132	W14X132	W14X90	W14X90	W14X82	W14X82
6-22-15	W14X132	W14X132	W14X90	W14X90	W14X82	W14X82
6-22-30	W14X145	W14X145	W14X132	W14X132	W14X120	W14X120

4. Numerical Models

In accordance with the P-695, models were developed using expected material properties and behavior, so that results will represent the median response of the building. *OpenSees*, an open source finite-element modeling software developed for earthquake simulations, was used for modeling (*OpenSees* commands in italics) [15].

4.1 Buckling Restrained Braces

The braces were modeled as single *corotTruss* elements, with effective properties to account for the non-prismatic geometry of BRBs [16]. The yield stress of the core was assumed to be 42 ksi (290 MPa), the assumed median yield stress of the acceptance range, and ultimate stresses were taken as the adjusted strength stresses. The *Steel4* material was used with typical parameters for A36 steel BRBs [17], and the *Fatigue* wrapper material was used to enforce a rain-counting damage limit state as well as a core tensile rupture strain of 4%, which corresponds to a ductility demand of approximately 30 [18, 19].

4.2 Post-tensioning (PT)

PT elements were modeled as tension-only *truss* elements with an initial strain corresponding to the target stress. Post-yield stiffness was assumed to be zero, and a tensile strain limit of 5% was imposed on the elements to simulate tensile strand fracture [20]. To address strain losses due to elastic axial shortening of frame elements, an automated procedure was developed within the *OpenSees* framework that applied the initial PT force to the reacting elements before adding the PT elements.

4.3 Boundary Frame Elements

Although the proposed system was designed to remain elastic at the design level drift, yielding of the beams and columns was directly modeled to capture collapse-level behavior. The beams and columns were modeled as *forceBeamColumn* elements with fiber sections. Fibers were modeled with a *Steel01* material with a yield stress equal to 55 ksi (379 MPa) and 2% kinematic strain hardening. Beam-column connections were modeled with an *equalDOF* constraint for the shear plate and a compression-only spring *truss* element for the top-flange contact. Gravity loads on the boundary frame elements were taken to be the P-695 load combination of 1.05 dead load and 0.25 live load, and second order effects were incorporated through use of *P*-delta leaning columns on both sides of the frame.

5. Non-Linear Static Analysis

Non-linear static (pushover) analyses were conducted on each of the eight models, using a first-mode shape force distribution, and an assumed rightward drift condition. The pushover curves were used to establish both the overstrength factor Ω and the period-based ductility μ_T for each model. A soft-story mechanism, caused by rupture of the first floor BRB core, was observed at the first floor, especially for the 6-story models. This was reflected with smaller period-based ductilities for the 6-story models. The period-based ductility and overstrength parameters determined from the pushover analyses are summarized in Table 5.

Table 5 – Non-Linear Static Pushover Analysis Results

3-Stories			6-Stories		
ID	**Ω**	**μ_T**	**ID**	**Ω**	**μ_T**
3-14-15	1.55	4.59	6-14-15	1.39	3.18
3-14-30	1.66	4.32	6-14-30	1.43	3.02
3-22-15	1.69	4.34	6-22-15	1.45	2.94
3-22-30	1.94	3.54	6-22-30	1.54	2.90

6. Non-Linear Response-History Analysis

Non-linear response-history analyses were conducted on the eight prototype buildings with the P-695 far field ground motion suite, listed in Table 6. Following the P-695, the suite was normalized to the median of the geometric mean of peak ground velocity, or PGV_{PEER}, and the median spectra of the normalized ground motion suite was used for anchoring to the DBE and MCE response spectra. The normalization factors for the suite are published in the P-695, but the factors were developed using an older version of the NGA database [21]. Accordingly, updated ground motion records were acquired from the NGA-West2 and CESMD databases [22] and new normalization factors were computed. A comparison of the values listed in the P-695 and the new values is shown in Table 6.

Table 6 –Ground Motion Suite and Normalization Factors [5]

Ground Motion		**Normalization Factor**	
ID	**Name**	**P-695**	**Computed**
1	Northridge – Beverly Hills - Mulhol	0.65	0.64
2	Northridge – Canyon Country-WLC	0.83	0.94
3	Duzce, Turkey – Bolu	0.63	0.66
4	Hector Mine – Hector	1.09	1.18
5	Imperial Valley – Delta	1.31	1.37
6	Imperial Valley – El Centro Array #11	1.01	1.01
7	Kobe, Japan – Nishi-Akashi	1.03	0.95

8	Kobe, Japan – Shin-Osaka	1.10	1.54
9	Kocaeli, Turkey – Duzce	0.69	0.70
10	Kocaeli, Turkey – Arcelik	1.36	1.71
11	Landers – Yermo Fire Station	0.99	1.05
12	Landers – Coolwater	1.15	1.17
13	Loma Prieta – Capitola	1.09	1.20
14	Loma Prieta – Gilroy Array #3	0.88	0.99
15	Manjil, Iran – Abbar	0.79	0.87
16	Superstition Hills – El Centro Imp. Co.	0.87	0.90
17	Superstition Hills – Poe Road (temp)	1.17	1.17
18	Cape Mendocino – Rio Dell Overpass	0.82	0.92
19	Chi-Chi, Taiwan – CHY101	0.41	0.48
20	Chi-Chi, Taiwan – TCU045	0.96	0.84
21	San Fernando – LA - Hollywood Stor FF	2.10	2.10
22	Friuli, Italy – Tolmezzo	1.44	1.53

It was determined that the new normalization factors differed from the originals by as much as 40%. The ground motion suite was normalized according to the computed factors, and the median spectra was used for anchoring the entire ground motion suite. The response spectra of the normalized suite of ground motions, as well as the median (in bold), are shown in Fig. 2.

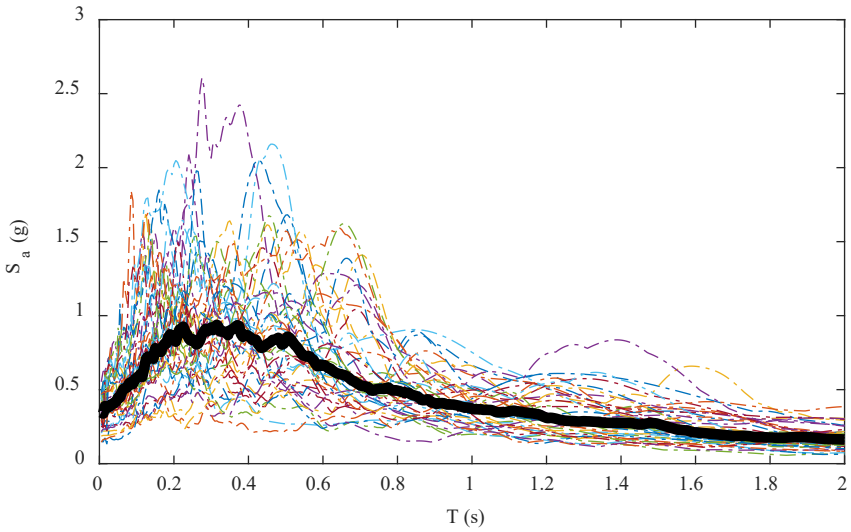

Fig. 2 – Response Spectra of Normalized P-695 Suite

To evaluate the DBE and MCE behavior of the NZ-BRB frame, each model was subjected to the normalized P-695 ground motion suite with the median spectra anchored at the approximate fundamental period DBE and MCE intensities. Individual response-history analyses were conducted at a time-step equal to 10% of the ground motion time-step and with 100 seconds of free vibration. Rayleigh damping of 2.5% was assumed and was applied to the boundary frame elements and braces with the *Region* command. The current-stiffness matrix was used in lieu of the initial stiffness matrix for Rayleigh damping, as initial-stiffness damping introduces artificial damping forces when elements soften [23]. Since using the current-stiffness matrix for damping can cause convergence issues with Newmark integrators, the Hilber-Hughes-Taylor integrator with $\alpha = 0.9$ was used [24]. Collapse was determined by either dynamic instability or non-simulated collapse

enforced during analysis. Since component softening and degradation were explicitly modeled, a global non-simulated collapse condition of 10% interstory drift was imposed [8, 25].

Peak interstory and roof drifts, as well as residual interstory and roof drifts, were recorded for each analysis. Mean (μ) and mean plus one standard deviation (μ+σ) quantities are reported for peak drifts in Table 7 and for residual drifts in Table 8. No collapses were observed at the DBE level, but collapses were observed at the MCE for about 2% of the 3-story models and about 8% of the 6-story models. Collapsed runs were excluded from the statistics in Table 7 and Table 8.

Table 7 – Peak Drifts

	Controlling Interstory Drift				Roof Drift			
	DBE		MCE		DBE		MCE	
ID	μ	μ+σ	μ	μ+σ	μ	μ+σ	μ	μ+σ
3-14-15	1.50%	2.12%	2.43%	3.56%	0.97%	1.33%	1.47%	2.05%
3-14-30	1.44%	2.03%	2.27%	3.27%	0.95%	1.32%	1.45%	2.03%
3-22-15	1.42%	1.99%	2.24%	3.20%	0.94%	1.30%	1.44%	2.01%
3-22-30	1.33%	1.87%	2.16%	3.04%	0.90%	1.27%	1.46%	2.05%
6-14-15	1.92%	2.78%	2.94%	4.39%	0.95%	1.33%	1.34%	1.78%
6-14-30	1.90%	2.79%	2.92%	4.36%	0.95%	1.32%	1.33%	1.79%
6-22-15	1.87%	2.73%	3.05%	4.60%	0.93%	1.29%	1.34%	1.80%
6-22-30	1.87%	2.77%	2.94%	4.29%	0.92%	1.29%	1.31%	1.73%

Table 8 – Residual Drifts

	Controlling Interstory Drift				Roof Drift			
	DBE		MCE		DBE		MCE	
ID	μ	μ+σ	μ	μ+σ	μ	μ+σ	μ	μ+σ
3-14-15	0.44%	0.81%	0.86%	1.68%	0.24%	0.45%	0.43%	0.86%
3-14-30	0.42%	0.75%	0.67%	1.27%	0.24%	0.46%	0.39%	0.78%
3-22-15	0.38%	0.68%	0.60%	1.12%	0.22%	0.41%	0.36%	0.70%
3-22-30	0.34%	0.60%	0.54%	1.01%	0.20%	0.38%	0.35%	0.69%
6-14-15	0.60%	1.27%	1.32%	2.49%	0.23%	0.48%	0.43%	0.78%
6-14-30	0.62%	1.29%	1.27%	2.47%	0.23%	0.48%	0.42%	0.78%
6-22-15	0.56%	1.20%	1.28%	2.52%	0.21%	0.44%	0.40%	0.74%
6-22-30	0.57%	1.12%	1.08%	1.87%	0.21%	0.43%	0.36%	0.62%

The results from the DBE and MCE response-history analyses show that the NZ-BRB frame has slightly smaller peak and residual drifts compared to conventional BRBF systems [3, 4]. Furthermore, smaller peak and residual drifts were observed in most cases for models with more PT strands and more initial PT stress. The 6-story models experienced higher levels of interstory drift than the 3-story models, but the roof drift levels were comparable, highlighting the observed soft-story on the 6-story models.

7. Incremental Dynamic Analysis Results

To characterize the collapse fragility of the NZ-BRB frame, Incremental Dynamic Analyses were conducted on the eight models. Incremental Dynamic Analysis (IDA), developed by Vamvatsikos and Cornell [26], has been used as an assessment tool in earthquake engineering and research, and is required for a P-695 collapse study. Using the normalized ground motion suite, the IDAs were conducted using the *hunt & fill* tracing algorithm [26], utilizing a master-slave parallel processing scheme [27].

Individual analyses for the collapse study were conducted with 20 seconds of free-vibration. The collapse point for each ground motion was determined to be the last converged run before the lowest intensity collapse. Using the collapse points, the median collapse intensity $\hat{S}_{CT}$ was computed for each model, and the ratio of $\hat{S}_{CT}$ to the MCE spectral acceleration S_{MT} at the approximate fundamental period T_a was computed as the collapse margin ratio (CMR). Fig. 3 shows the interstory drift IDA plot for model 3-14-15.

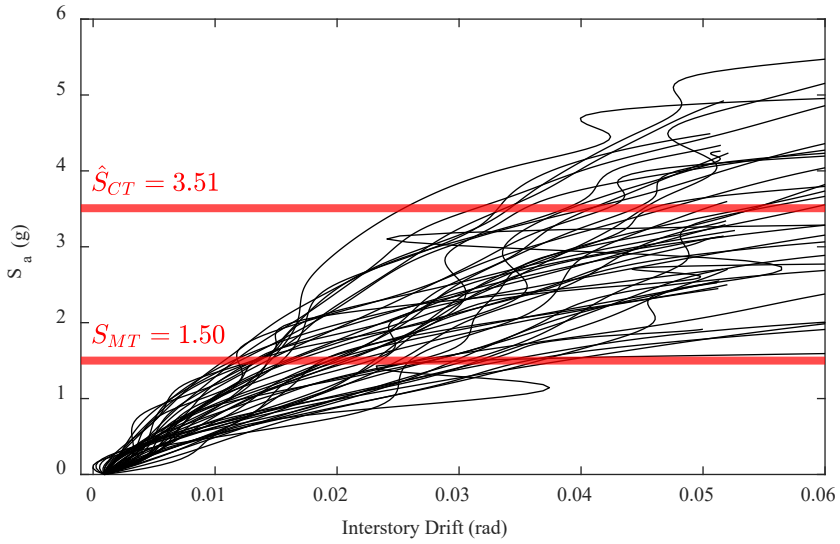

Fig. 3 – Interstory Drift IDA Plot for Model 3-14-15 (CMR = 2.34)

Collapse was observed to be primarily precluded by rupture of the first floor BRB, which is consistent with the sharp decline in capacity after BRB rupture shown in the non-linear static analyses. Collapse intensities for each ground motion were used to compute probabilities of collapse; probability of collapse at a specified intensity was taken to be the number of ground motions collapsing above the specified intensity, divided by the total number of ground motions. Using the calculated probabilities of collapse, lognormal fragility curves were developed, using maximum likelihood estimators [28]. Fig. 4 and Fig. 5 show the computed collapse fragility curves.

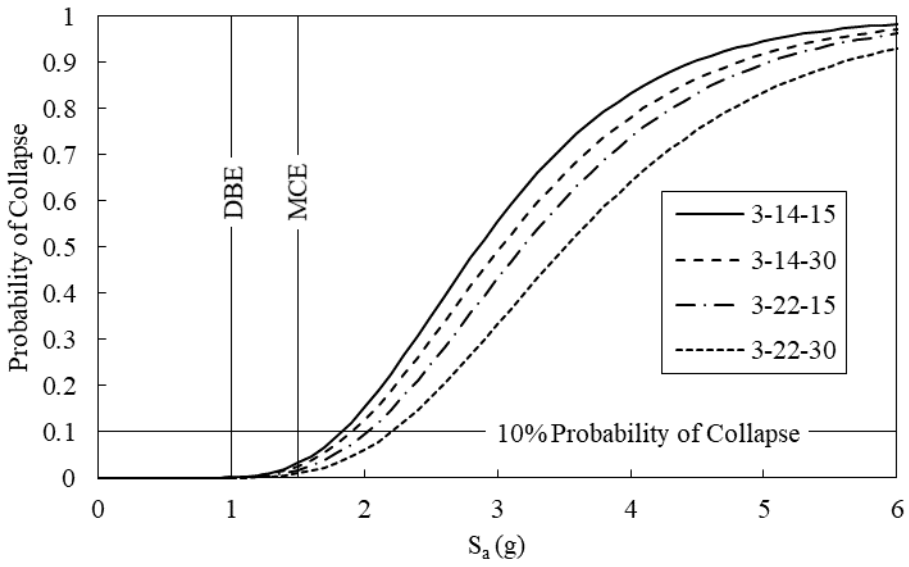

Fig. 4 – Collapse Fragility Curves: 3-Story Models

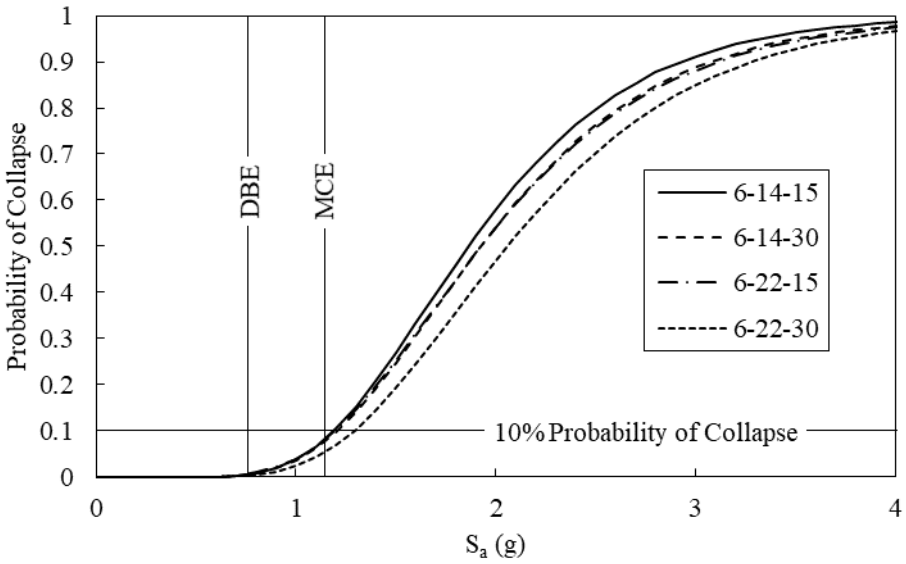

Fig. 5 – Collapse Fragility Curves: 6-Story Models

The fitted fragility curves are consistent with the observed collapse rates at the DBE and MCE levels, and the target 10% collapse at MCE was met for all models. The effect of the PT parameters is also consistent with the trends observed at the DBE and MCE levels: more PT generally leads to better performance. Furthermore, collapse capacity increased with the addition of more PT strands and stress.

In addition to developing collapse fragility curves, "self-centering fragility" curves were developed. Self-centering fragility was defined as the probability of self-centering at or below a given intensity measure, and self-centering was defined as having a residual interstory drift less than 0.2%, which is the out-of-plumb tolerance for new construction [29]. IDAs were conducted to determine the self-centering intensity measure, using 100 seconds of free-vibration for individual analyses. Probability of self-centering at a specified intensity was taken to be the number of ground motions self-centering at or above the specified intensity, divided by the total number of ground motions. Lognormal fragility curves were fit to the results for the ground motion suite, and are shown in Fig. 6 and Fig. 7.

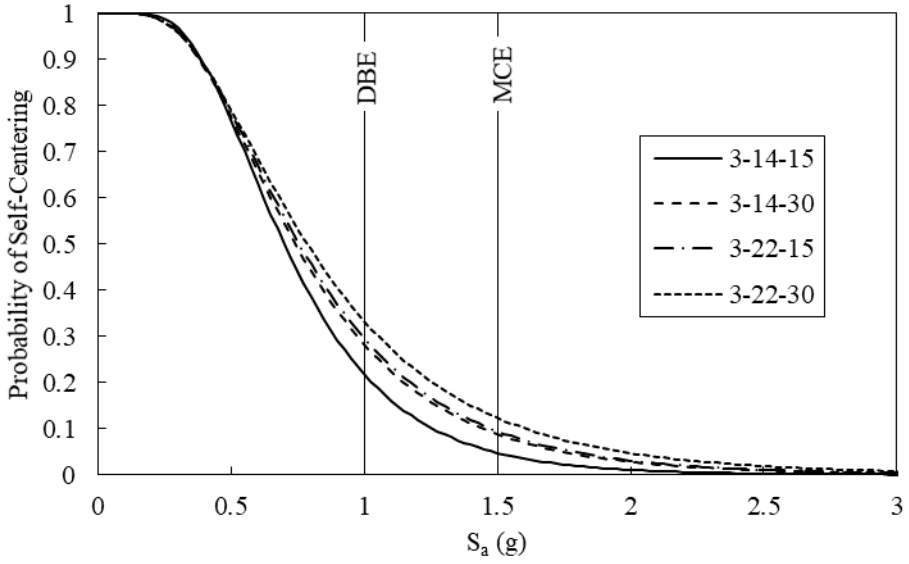

Fig. 6 – Interstory Drift Self-Centering Fragility: 3-Story Models

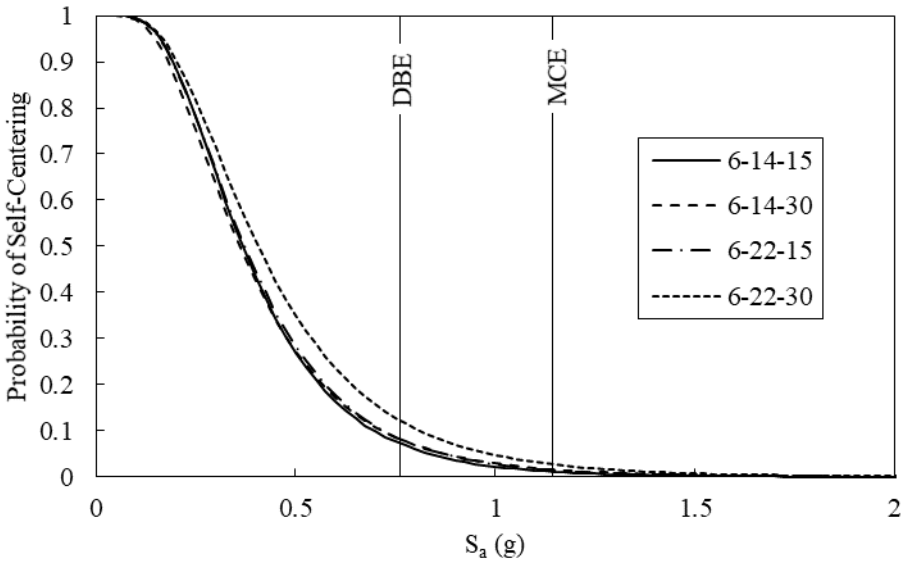

Fig. 7 – Interstory Drift Self-Centering Fragility: 6-Story Models

The effect of the PT parameters was similar to trends in Table 8: PT strands and initial stress generally increased the probability of self-centering, especially for the 3-story models. The effect of PT parameters on self-centering fragility was not as clear for the 6-story models. From the preliminary results, it is suspected that keeping the PT the same at each floor may have led to proportionally stiffer upper floors. Using PT configurations proportional to story stiffness may reduce the observed soft-story effects and help with self-centering.

8. P-695 Performance Evaluation

Although the fitted IDA collapse fragility curves passed the target of 10% collapse at MCE, the system did not pass the P-695 performance evaluation. The P-695 performance evaluation assumes a lognormal fragility curve centered on the adjusted collapse margin ratio (ACMR), which is the CMR adjusted for amplitude scaling bias, and with a lognormal standard deviation (β factor) representing both the record-to-record variability and the variability due to confidence and completeness of the study. The assumed quality rating scores and corresponding β factors are summarized in Table 9.

Table 9 – Assumed P-695 Quality Ratings

Category	Completeness	Confidence	Rating	β
Design Requirements	Medium	Medium	Fair	0.35
Test Data	Low	Medium	Poor	0.5
Index Archetype Models	Low	High	Fair	0.35

ACMRs and acceptable ACMRs for the target 10% collapse at MCE ($ACMR_{10\%}$) were computed for each model in accordance with the P-695. The ACMRs ranged from 2.00 to 2.81 and the $ACMR_{10\%}$ ranged from 2.81 to 2.82 for the eight prototype buildings. None passed the acceptance criteria. For P-695 verification, greater certainty would have to be achieved and/or a smaller *R*-factor would have to be used.

9. Conclusions

Preliminary numerical results of the proposed NZ-BRB frame, which combines BRB structural fuses with a PT rocking boundary frame, demonstrate that it exhibits comparable behavior to conventional BRBF systems. Results from a limited parametric study on the PT parameters show that greater self-centering capability, as well as collapse capacity, can be achieved by increasing the robustness of the PT boundary frame. Failure of the proposed system was observed to be primarily due to a first-floor soft-story and BRB rupture. Although the assumed *R*-factor was not validated through the P-695 performance evaluation for the select prototype buildings, the IDA collapse fragility curves show promise for the system and inform a more detailed P-695 study.

10. References

[1] ASCE, *Minimum Design Loads for Buildings and Other Structures, ASCE 7-05*. 2005, Reston, VA: American Society of Civil Engineers.

[2] AISC, *Seismic Provisions for Structural Steel Buildings, AISC 341-05*. 2005, Chicago, IL: American Institute of Steel Construction.

[3] Fahnestock, L., R. Sause, and J. Ricles, *Seismic Response and Performance of Buckling-Restrained Braced Frames.* Journal of Structural Engineering, 2007(9): p. 1195-1204.

[4] Sabelli, R., S. Mahin, and C. Chang, *Seismic demands on steel braced frame buildings with buckling-restrained braces.* Engineering Structures, 2003. **25**(5): p. 655-666.

[5] FEMA, *Quantification of Building Seismic Performance Factors, FEMA P-695*. 2009, Washington, D. C.: Federal Emergency Management Agency.

[6] Dowden, D.M. and M. Bruneau, *Kinematics of Self-Centering Steel Plate Shear Walls with NewZ-BREAKSS Post-Tensioned Rocking Connection.* Engineering Journal-American Institute Of Steel Construction, 2016. **53**(3): p. 117-135.

[7] ASCE, *Minimum Design Loads and Associated Criteria for Buildings and Other Structures, ASCE/SEI 7-16*. 2016, Reston, Virginia: American Society of Civil Engineers.

[8] NEHRP, *Evaluation of the FEMA P-695 Methodology for Quantification of Building Seismic Performance Factors*. 2010.

[9] FEMA, *State of the Art Report on Systems Performance of Steel Moment Frames Subject to Earthquake Ground Shaking, FEMA 355C*. 2000, Washington, D.C.: Federal Emergency Management Agency.

[10] Pham, H., *Performance-based assessments of buckling-restrained braced steel frames retrofitted by self-centering shape memory alloy braces*, in *Civil and Environmental Engineering*. 2013, Georgia Institute of Technology.

[11] Dowden, D.M., P.M. Clayton, C.-H. Li, J.W. Berman, M. Bruneau, L.N. Lowes, and K.-C. Tsai, *Full-Scale Pseudodynamic Testing of Self-Centering Steel Plate Shear Walls.* Journal of Structural Engineering, 2016. **142**(1).

[12] NIST, *Seismic design of steel buckling-restrained braced frames: A guide for practicing engineers*. 2015, GCR 15-917-34, NEHRP Seismic Design Technical Brief No. 11, produced by the Applied Technology Council and the Consortium of Universities for Research in Earthquake Engineering for the National Institute of Standards and Technology, Gaithersburg, MD.

[13] AISC, *Seismic Provisions for Structural Steel Buildings, AISC 341-16*. 2016, Chicago, IL: American Institute of Steel Construction.

[14] Robinson, K., *Specifying Buckling-Restrained Brace Systems.* Modern Steel Construction, 2009. **49**(11): p. 57-57.

[15] McKenna, F.T., *OpenSees*. 1999, University of California Berkeley.

[16] Tremblay, R., L. Poncet, P. Bolduc, R. Neville, and R. Devall. *Testing and Design of Buckling Restrained Braces for Canadian Application*. in *13th World Conference on Earthquake Engineering*. 2004. Vancouver, B.C., Canada.

[17] Zsarnóczay, Á., *Experimental and Numerical Investigation of Buckling Restrained Braced Frames for Eurocode Conform Design Procedure Development*, in *Department of Structural Engineering*. 2013, Budapest University of Technology and Economics.

[18] Speicher, M.S. and J.L. Harris, *Collapse Prevention seismic performance assessment of new buckling-restrained braced frames using ASCE 41.* Engineering Structures, 2018. **164**(C): p. 274-289.

[19] Zaruma Ochoa, S.R., *Seismic stability of buckling-restrained braced frames*, in *Civil & Environmental Eng*. 2017, University of Illinois at Urbana-Champaign.

[20] Ravi K. Devalapura, M.K.T., *Stress-Strain Modeling of 270 ksi Low-Relaxation Prestressing Strands.* PCI Journal, 1992. **37**(2): p. 100-106.
[21] Ancheta, T., R. Darragh, J. Stewart, E. Seyhan, W. Silva, B. Chiou, K. Wooddell, R. Graves, A. Kottke, D. Boore, T. Kishida, and J. Donahue, *NGA-West2 Database.* Earthquake Spectra, 2014. **30**(3): p. 989-1005.
[22] COSMOS. *Center for Engineering Strong Motion Data*. [cited 2019 Jan 31]; Available from: https://strongmotion.org/Projects/CESMD/.
[23] Charney, F., *Unintended Consequences of Modeling Damping in Structures.* Journal of Structural Engineering, 2008(4): p. 581-592.
[24] Hilber, H.M., T.J.R. Hughes, and R.L. Taylor, *Improved numerical dissipation for time integration algorithms in structural dynamics.* Earthquake Engineering & Structural Dynamics, 1977. **5**(3): p. 283-292.
[25] FEMA, *Recommended Seismic Design Criteria for New Steel Moment-Frame Buildings, FEMA 350*. 2000, Washington, D.C.: Federal Emergency Management Agency.
[26] Vamvatsikos, D. and C.A. Cornell, *Incremental dynamic analysis.* Earthquake Engineering & Structural Dynamics, 2002. **31**(3): p. 491-514.
[27] Vamvatsikos, D., *Performing incremental dynamic analysis in parallel.* Computers and Structures, 2011. **89**(1): p. 170-180.
[28] FEMA, *Seismic Performance Assessment of Buildings, FEMA P-58*. 2018, Washington, D. C.: Federal Emergency Management Agency.
[29] AISC, *Code of Standard Practice for Steel Buildings and Bridges, AISC 303-16*. 2016, Chicago, IL: American Institute of Steel Construction.

